Representation Learning for Object Detection from Unlabeled Point Cloud Sequences

Xiangru Huang
MIT CSAIL
xrhuang@csail.mit.edu

Yue Wang[*]
NVIDIA Research & MIT CSAIL
yuewang@csail.mit.edu

Vitor Guizilini
Toyota Research Institute (TRI)
vitor.guizilini@tri.global

Rares Ambrus
Toyota Research Institute (TRI)
rares.ambrus@tri.global

Adrien Gaidon
Toyota Research Institute (TRI)
adrien.gaidon@tri.global

Justin Solomon
MIT CSAIL
jsolomon@mit.edu

Abstract: Although unlabeled 3D data is easy to collect, state-of-the-art machine learning techniques for 3D object detection still rely on difficult-to-obtain manual annotations. To reduce dependence on the expensive and error-prone process of manual labeling, we propose a technique for representation learning from unlabeled LiDAR point cloud sequences. Our key insight is that moving objects can be reliably detected from point cloud sequences without the need for human-labeled 3D bounding boxes. In a single LiDAR frame extracted from a sequence, the set of moving objects provides sufficient supervision for single-frame object detection. By designing appropriate pretext tasks, we learn point cloud features that generalize to both moving and static unseen objects. We apply these features to object detection, achieving strong performance on self-supervised representation learning and unsupervised object detection tasks. Code is available at `https://github.com/xiangruhuang/PCSeqLearning`

Keywords: Representation learning, object detection, point cloud sequences

Among the modalities used for object detection in autonomous driving, LiDAR point clouds capture accurate 3D scene structure, yielding state-of-the-art performance [1, 2]. Yet, sparsity and irregularity make it difficult for models to generalize to complicated real-world environments. Moreover, object detection requires several tasks to be solved jointly, including foreground–background segmentation, instance segmentation, object localization, and classification. This results in a high demand for human labels of object locations, velocities, orientations, and other properties.

Unlike expensive human-generated labels, *unlabeled* point cloud sequences can easily be collected by autonomous vehicles with LiDAR sensors whenever they are on the road. These temporally-ordered sequences contain more information than individual frames. For example, we can estimate correspondences between adjacent point clouds. Recent works distill information learned from point cloud sequences to train single-frame models for motion estimation, object detection, prediction, and motion tracking [3, 4, 5, 6, 7, 8, 9, 10, 11]. These works typically focus on a sub-module relevant to object detection (e.g., scene flow), or require many labeled sequences to promote generalization.

We propose a representation learning approach to learning features for object detection from unlabeled LiDAR point cloud sequences. Unlike previous works, ours is capable of learning features without 3D bounding box annotations, with competitive performance on object detection benchmarks among unsupervised and self-supervised approaches. To deliver generalization from limited labeled data, we use geometry processing techniques to derive a pseudo-label generator. This generator ingests unlabeled point cloud sequences and produces annotations for pretext tasks like motion segmentation and moving object detection. Then, we use the generated annotations to pretrain a *single-frame* feature extractor that can be used for downstream tasks like object detection.

Our pseudo-label generator identifies moving objects as sequences of point clusters across frames (Figure 2). Unlike existing single-frame LiDAR segmentation methods that focus on point connectivity [12, 13, 14], we estimate motion and planar structures from each sequence. This information

[*]Work done while at MIT.

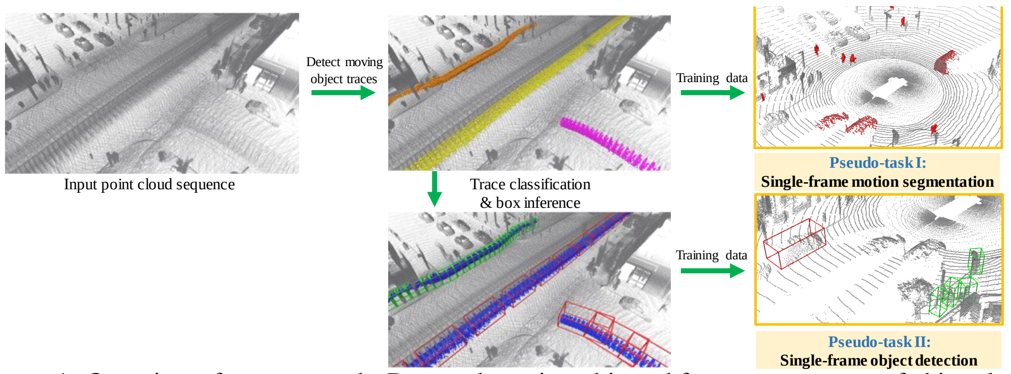
Input point cloud sequence
Detect moving object traces
Trace classification & box inference
Training data
Training data
Pseudo-task I:
Single-frame motion segmentation
Pseudo-task II:
Single-frame object detection
Figure 1: Overview of our approach. Detected moving objected from sequences are fed into later self-supervised tasks.

enables us to separate out moving objects reliably, yielding highly-accurate moving object detection. By combining all detected point clusters in the sequence, we further estimate the location, orientation, and category of each moving object. To promote generalization and mitigate the bias of working exclusively with moving objects, we propagate estimated pseudo-labels to static objects following a variant of [11]. The key difference of our approach is that we check the consistency of predicted object labels across frames to prune incorrect predictions, improving robustness of label propagation.

To summarize, our contributions are as follows:

- An algorithm for the detection of moving objects from unlabeled point cloud sequences, which enables self-supervised representation learning for point cloud data.
- Two representation learning pseudo-tasks leveraging our detected moving objects for the downstream task of object detection, without requiring manually-annotated labels at any stage of training.
- Competitive self-supervised object detection accuracy and state-of-the-art unsupervised object discovery accuracy.

1 Related Work

Point cloud self-supervised learning. Self-supervision is popular for representation learning from unlabeled data. For point clouds, several self-supervised pretext tasks have been proposed. Sauder and Sievers [15] split point clouds into voxels and reassemble shuffled voxels. Zhang et al. [16] enforce consistency between point cloud and voxel representations. Xie et al. [17] synthesize transformed point clouds and enforce consistency. P4Contrast uses point-pixel pairs to learn complementary features from point clouds and images [18]. Liu et al. [19] include negative pairs in P4Contrast. Tian et al. [20] learn to discover unseen objects from image and LiDAR clues. Our work is closely related to representation learning and unsupervised object discovery method, using relationships between adjacent frames to augment available information.

3D object detection. 3D object detection works can be categorized by data type, e.g. voxels [21], points [22, 23], range images [24, 25], and hybrid representations [26, 27, 28]. Many works incorporate temporally-adjacent frames to improve detection. Luo et al. [29] stack frames into a sparse 4D tensor, using 3D convolutions for efficiency. Hu et al. [30] incorporate temporal voxel occupancy estimated from raycasting. Several models deal with spatio-temporal information, such as Transformers [31] and LSTMs [32]. Ku et al. [33], Chen et al. [34], Xu et al. [35] combine modalities like point clouds and images into a single framework. Frustum-PointNet leverages 2D object detectors to form a frustum crop of points and then uses PointNet to aggregate features [36]. Beyond visual input, Yang et al. [37] use high-definition maps to boost performance of 3D object detectors. Liang et al. [38] argue that multi-tasking improves representations over single-tasking. Our method is also closely related to [39], which learns a perceptual model for unknown classes.

Learning from point cloud sequences. Point cloud sequence datasets have grown in scale and diversity, covering tasks like 3D reconstruction [40, 41], semantic segmentation [42], and object detection [1, 2, 43]. Although sequences often yield better performance than single frames, they require new representations. Early works treated them as 4D grids [44]. MeteorNet includes spatio-temporal neighborhoods for dynamic point cloud sequences [45]. CaSPR normalizes the temporal dimension [9], yielding a time-continuous representation. Mersch et al. [5] convert point sequences

	Car	Pedestrian	Cyclist
Box Count	4352210	2037627	49518
Moving Box Count	1161019	1427211	42411
Moving Trace Count	12496	13052	438
Velocity in $[0.05, 2]$ m/s	850640	1044324	37051
Turning Angle $< 3^\circ$	1153865	1379915	41546

Table 1: Waymo Open training dataset statistics [1] (798 sequences), including the number of (moving or all) bounding boxes, the number of unique moving objects and the velocity and turning angle distribution of all moving bounding boxes. We focus on the fraction of moving boxes that follow a smooth trajectory.

into stacked 2D range images, processed using 3D convolution. Qi et al. [11] use motion and complementary views to help detect moving and static objects. Compared to previous work, our approach performs object detection without requiring annotated 3D bounding boxes.

2 Approach Overview

Our framework takes two main steps, summarized in Figure 1: (1) extract a set of moving objects (defined below as *object traces*) from a temporally-ordered sequence of unlabeled point clouds; and (2) train a feature extraction module using these object traces. We do *not* require human-labeled 3D bounding boxes at any stage. Here, we introduce the concept of object traces and discuss why they are necessary for our approach. We then elaborate the key observations and challenges in each step.

Object traces. Point cloud segmentation generally involves finding instances of objects, represented by sets of point clusters $\{C_i\}$ where $C_i \in \mathbb{R}^{M_i \times 3}$. In point cloud sequences, object instances appear consistently in consecutive frames. Therefore, we are interested in *object traces*, which are sequences of point clusters across consecutive frames corresponding to the same object.

Formally, given a point cloud sequence $\mathcal{P} = \{P_1, \dots, P_N\}$ where P_t is the t-th frame from a LiDAR camera, an *object trace* is a temporally-ordered sequence of clusters $\mathcal{C} = \{C_l, \dots, C_r\}$, where $C_t \subseteq P_t$ for any $1 \le l \le t \le r \le N$. Figure 2 shows an example.

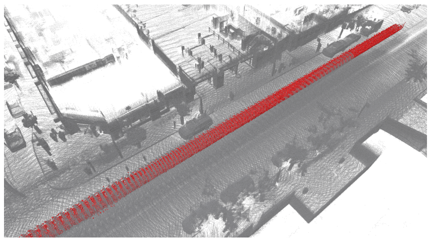
Figure 2: An *object trace* is a sequence of point clusters moving along a smooth trajectory. Here, we highlight an object trace of a moving vehicle.

Our key observation is that many object classes relevant for autonomous driving are *dynamic*, including pedestrians, vehicles, and cyclists. Statistics from the Waymo dataset show that many ground truth object traces follow smooth trajectories (Table 1). Intuitively, the length and motion consistency of object traces reduce uncertainty in their detection, enabling our robust non-learning trace detection algorithms from unlabeled sequences. Detected traces can be used in subsequent pseudo-tasks.

Object trace detection. Detecting object traces is inevitably disturbed by interactions between objects and the environment and irregular motion and sampling density across frames. Even supervised methods suffer from detection uncertainty. Here, we focus on objects moving along smooth trajectories. Our detector optimizes for detection precision instead of coverage. This choice only adds a mild bias to the detected objects since velocities are independent from geometric appearance.

Our object trace detection follows a standard proposal-and-rejection framework. For each sequence, we propose candidate clusters corresponding to movable objects. Then, Kalman filtering acquires object traces according to their motion. We collect a subset of object traces with smooth trajectories.

Self-supervision. Given our high-quality detected object traces from unlabeled point cloud sequences, we design two self-supervised tasks that enable representation learning for point clouds.

The rest of our paper is organized as follows. §3 details our object trace detection algorithm. §4 introduces self-supervised tasks using detected object traces. §5 shows results on object trace detection and representation learning for object detection. §6 concludes and suggests future directions.

3 Object Trace Detection

Our object trace detection algorithm involves three steps: (1) preprocessing, (2) object cluster proposal, and (3) object trace tracking. We elaborate each step below.

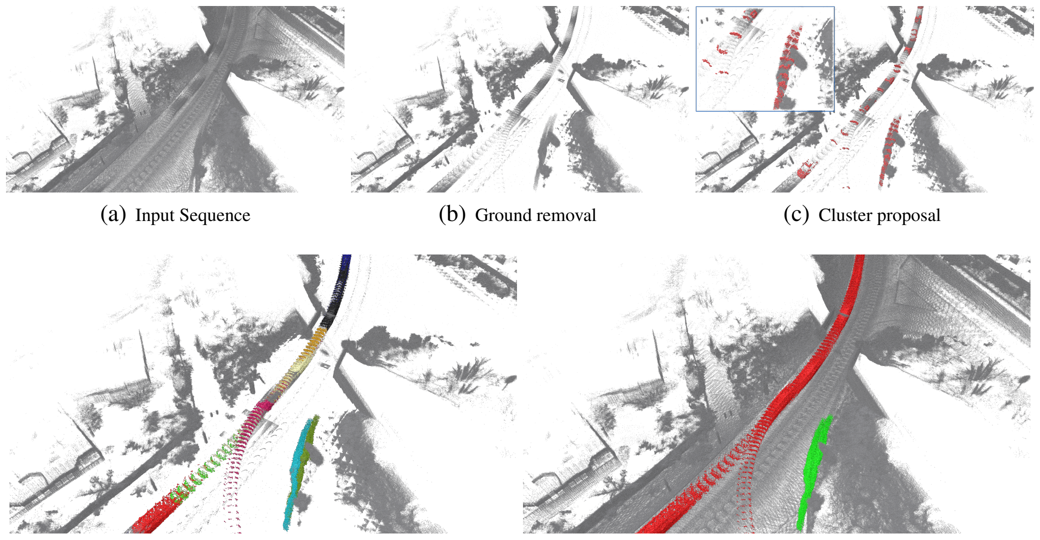

Figure 3: Object trace detection. In (a), we visualize the input point cloud sequence in world coordinates. Figures (b) to (d) show steps of trace detection. In (c), we highlight a subset of proposed object clusters in red. In (d), we color each detected trace differently. In (e), we visualize the ground truth, where vehicles are red and pedestrians are green.

Sequence preprocessing. We apply two preprocessing steps on each point cloud sequence before passing it to our detection algorithm. First, we bring all frames into the world coordinate system using the provided ego-motion (Figure 1, left). Second, we remove points on the ground, which typically account for 50% to 90% of the points; this improves detection efficiency and robustness. Appendix A provides preprocessing details.

Object cluster proposal. Since object sizes vary across classes, we use point cloud segmentation to extract point clusters corresponding to object instances. Unlike existing LiDAR point cloud segmentation methods, e.g. [13], we only extract segments corresponding to moving object instances.

Given a point cloud sequence, we use motion as a cue for segmentation. We estimate the velocity $\boldsymbol{v}_i \in \mathbb{R}^3$ of each point $\boldsymbol{p}_i$ and compute a pairwise proximity score s_{ij} via

$$s_{ij} = \exp\left(-\frac{\|\boldsymbol{p}_i - \boldsymbol{p}_j\|^2}{\sigma_p^2} - \frac{\|\boldsymbol{v}_i - \boldsymbol{v}_j\|^2}{\sigma_v^2}\right), \tag{1}$$

where $\sigma_p = 0.5$ m and $\sigma_v = 10$ m/s. σ_v is chosen to be large to reduce variance in velocity estimation. We then run normalized cuts [46] with edge weights $\{s_{ij}\}$ and select clusters with average velocity > 0.1 m/s and belong to the same frame.

To estimate motion, we adapt two state-of-the-art methods to point cloud sequences (details in §5). Our first variant "NeuralSF" follows Li et al. [47]. To accommodate point cloud sequences, we optimize for a spatiotemporal velocity field $f_\theta : \mathbb{R}^4 \rightarrow \mathbb{R}^3$ mapping any point location $\boldsymbol{x} \in \mathbb{R}^3$ and time t to a velocity $\boldsymbol{v} \in \mathbb{R}^3$. We normalize $(\boldsymbol{x}, t)$ to $[0, 1]^4$ and optimize network parameters θ using chamfer distance between adjacent frames. Our second alternative "SSL-SceneFlow" follows Mittal et al. [48], who estimate scene flow between adjacent frames. They train using self-supervision on KITTI and nuScenes. We apply their pretrained model to each pair of adjacent frames.

Object trace tracking. Assuming each point cluster rigidly transforms across frames, we adopt a multi-object tracking algorithm using Kalman filtering to track cluster motion [49]. Specifically, we use a Kalman filter to track the velocity of each object's center from a sequence of centers. For each cluster, if tracking succeeds, the output of tracking is a trace (§2). Appendix B provides details.

4 Self-Supervised Tasks

Given a set of object traces from moving object instances in LiDAR sequences, we design self-supervised tasks that yield point cloud features for downstream tasks like single-frame object detection.

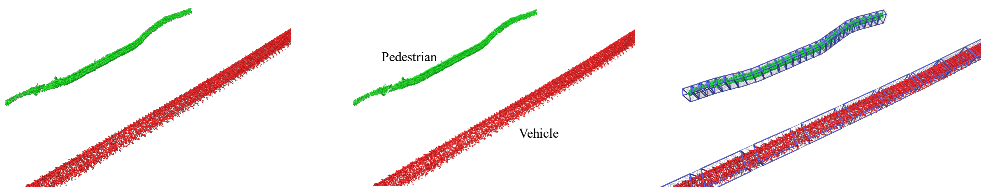

(a) Input object traces (b) Trace Classification (c) Box inference

Figure 4: Box inference. For visualization, (c) highlights the estimated bounding boxes.

Here we introduce two self-supervised tasks in §4.1 and §4.2, used to train a feature extractor with single-frame point cloud input. §4.3 provides details of our feature extraction module.

4.1 Task I: Motion Segmentation

We consider motion segmentation as the first self-supervised task. Since we extract traces with high precision, we can use them as segmentation masks to train a single-frame model differentiating moving objects from the background. We train a pointwise classifier that classifies each feature vector as either *moving* or *non-moving*, implemented as a multi-layer perceptron (MLP) combining ReLU [50] and BatchNorm [51] layers beyond the architecture in §4.3. Our loss is negative log-likelihood.

To generalize from moving to static objects, we augment each scene with randomly-sampled point clusters corresponding to moving objects from other scenes. In particular, for each scene, we randomly choose 50 point clusters and place them at a random locations.

4.2 Task II: Object Detection

Task I is straightforward but fails to use all available information. For example, object orientations can be inferred from motion but are ignored. Here, we estimate 3D bounding boxes and class labels from each object trace and use this information to train a 3D object detector; see Figure 4. We use the same box regression component and regression/classification loss as Yin et al. [52]. Estimating 3D bounding boxes to train the object detector from traces involves several subproblems:

- **Registration:** We estimate the velocity of each object cluster in each trace while enforcing smoothness. This enables us to approximately reconstruct the object by incorporating geometry collected from multiple frames.
- **Trace classification:** We categorize each object trace into one of the movable object classes. This is the only sub-problem that requires labeled data. We emphasize that class label is much cheaper to acquire compared to 3D bounding box annotations.
- **3D bounding box estimation:** Given estimated object class labels, we estimate the 3D bounding boxes for each object class. We propagate the box size estimate from densely reconstructed objects to sparse objects in each single frame, since the former provide high-confidence estimates.

The end result of the procedure above is a set of 3D bounding boxes that can be used to train a single-frame object detector. Details of these steps are provided below.

Registration. As observed in Table 1, most objects in the Waymo dataset follow smooth trajectories. For robustness against irregular sampling of LiDAR point clouds, we use this property to help estimate a velocity $\boldsymbol{v}_i \in \mathbb{R}^3$ for each object cluster C_i of frame i. We optimize

$$\min_{\boldsymbol{v}_i} \sum_{\substack{(i,j): \\ |i-j|=1}} \left(\lambda \|\boldsymbol{v}_i - \boldsymbol{v}_j\|^2 + \sum_{\boldsymbol{p} \in C_i} \frac{1}{|C_i|} \min_{\boldsymbol{q} \in C_j} \|\boldsymbol{p} + \boldsymbol{v}_i - \boldsymbol{q}\|^2 \right), \tag{2}$$

where $\lambda = 1$. The estimated $\{\boldsymbol{v}_i\}$ brings all object points to the same coordinate system, forming a denser point cloud of the object instance, enabling trace classification and 3D box estimation.

Trace classification. Since object class labels are semantic rather than geometric, some minimal supervision is needed to distinguish classes (car, pedestrian, cyclist). We extract ground truth object class labels for 1,500 object instances (600 cars, 600 pedestrians and 300 cyclists) out of around 8 millions object instances (or 26,000 object traces) in our training dataset to train an object classifier

	Vehicle				Pedestrian				Cyclist			
	IoU=0.6		IoU=0.7		IoU=0.4		IoU=0.5		IoU=0.4		IoU=0.5	
	L1 AP	L2 AP	L1 AP	L2 AP	L1 AP	L2 AP	L1 AP	L2 AP	L1 AP	L2 AP	L1 AP	L2 AP
Ours-LP1	17.5	17.0	6.1	5.9	28.4	26.2	21.2	19.6	59.9	57.8	48.5	46.8
Ours-LP2	43.7	39.6	15.1	13.8	45.6	40.1	31.6	27.2	63.7	61.2	49.7	47.3
Ours-no-seg	52.8	47.8	21.4	19.3	51.4	45.4	32.9	28.0	63.3	60.7	48.7	46.3
Ours	53.6	48.8	22.3	20.6	51.6	45.9	33.7	28.9	64.6	62.0	50.1	47.6

Table 2: Single-frame object detection results for unsupervised learning approaches. Here LP1/LP2 stands for the trained model before the first/second iteration of label propagation.

that takes an object trace and outputs an object class label. An additional object class "Other" is included to deal with outliers. We label 3,000 instances of outliers as "Other". Our object trace classifier is adapted from Point Transformer [53] and Voxel-based architectures, with 5 transition-down layers of dimension 32, 64, 128, 256, and 256, respectively. Each trace is represented as a 4D matrix with each row representing the location and time of a point.

Bounding box estimation. In LiDAR object detection, each 3D bounding box is represented by a 7D vector with location, size, and orientation. Since object sizes vary among classes, we group object traces based on the estimated object class labels. For each object class, we observe that there is a fraction of objects that are densely captured by LiDAR while the rest only represent object parts.

Therefore, we learn a model that regresses the bounding box size for each object trace, assuming it does not change along each trace. For each class, we select the top 20% of object traces ranked by number of points. We then use the velocity computed in (2) to bring point clusters into the same coordinate system and compute a 3D bounding box that covers all points with minimal volume. The resulting bounding box size vectors are used to train a model that regresses bounding box size. We use the model to predict bounding box sizes from all other object traces. The model architecture and input data representation of the regression model are also adopted similarly as in trace classification.

Given the box size, we solve an optimization problem to estimate box location and orientation:

$$\min_{\boldsymbol{b}_i} \sum_{(i,j):|i-j|=1} d_1(\boldsymbol{b}_i, \boldsymbol{b}_j) + d_2(\boldsymbol{b}_i, C_i). \tag{3}$$

Here, $\boldsymbol{b}_i$ represents box attributes, d_1 penalizes differences in orientation and enforces smoothness of box locations, and d_2 encourages the i-th box $\boldsymbol{b}_i$ to cover the i-th point cluster C_i. See appendix C.

Moving-to-static label propagation. The resulting 3D bounding boxes only represent moving objects in each sequence. To promote generalization, we notice that static clusters of movable objects can be extracted but were rejected in the object cluster tracking step (see section 3). We train a classifier on *registered* object traces and ask it to find out static clusters that are geometrically similar. In addition, we train a single-frame object detector using estimated 3D bounding boxes and apply it to predict 3D bounding boxes on the training data. Due to the geometric similarity between moving and static objects, the object detector generates 3D bounding boxes for static objects. To improve robustness, we then apply [49] to verify consistency of temporally-adjacent bounding boxes and reject false positives. The verified 3D bounding boxes for static objects are added to the training set to train another single-frame object detector from scratch. We repeat this procedure twice, yielding a single-frame object detector that reasonably generalizes to moving and static objects. Appendix D provides details and visualization.

4.3 Model Architecture

We modify the CenterPoint architecture [54, 52] to construct our single-frame feature extractor, which outputs a 256-dimensional feature for each 2D grid cell of size $0.1\text{m} \times 0.1\text{m}$ in the x-y plane. The architecture is identical to the "VoxelNet" variant of CenterPoint that uses the SpConv Library for feature extraction [55]. The bounding box regression layer is modified according to self-supervised tasks discussed later. The training parameters are set to the same as the Waymo dataset defaults.

5 Experiments

We perform experiments related to each step of our proposed approach. Unlike most self-supervised learning works that require fine-tuning on labeled data, our self-supervised tasks are closer to the

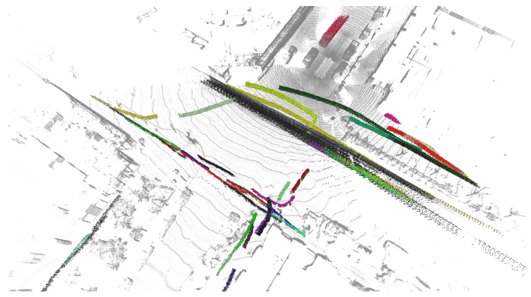
(a) Detected Object Traces

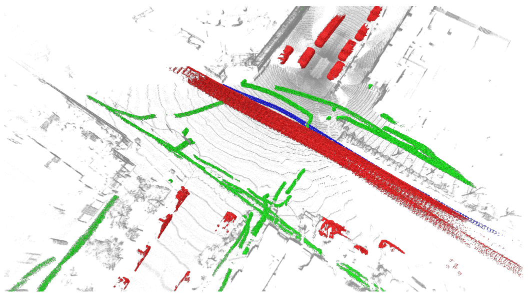
(b) Ground Truth Object Points

Figure 5: Qualitative results of our detected object traces. Left: Results of our object trace detection algorithm, each object trace is in different color. Right: Ground truth points corresponding to moving or static objects with different color (red: vehicle, blue: cyclist, green: pedestrian).

downstream tasks, enabling us to train a single-frame object detector with only a small set of class labels are needed but not any 3D box labels. We therefore perform two sets of evaluation on object detection algorithms, corresponding to the unsupervised setting and the self-supervised setting. In addition, we evaluate the quality of our detected object traces to demonstrate the reliability of our object trace detection algorithm.

§5.1 compares variants of our object trace detection algorithms in terms of the quality of the object traces. §5.2 compares our unsupervised single-frame object detector trained via self-supervised tasks described in §4 without any annotated 3D bounding boxes. §5.3 compares our single-frame object detector trained under different settings.

Dataset. We conduct our experiments on the Waymo Open Dataset for high-quality, dense point cloud sequences [1]. The dataset contains 798 training sequences and 202 validation sequences, with each sequence containing $\sim$200 frames with a sampling frequency of 10Hz.

5.1 Object Trace Detection Results

Here, we evaluate the quality of detected object traces using the methods in §3. We compare two algorithmics, NeuralSF and SSL-SceneFlow. Both adapt state-of-the-art scene flow estimation algorithms to point cloud sequences. We use the Waymo Open Dataset training split for both.

Evaluation protocol. We report the mean Intersection over Union (mIoU) between the detected object traces and the ground truth moving objects. For each detected point cluster, we find the 3D bounding box closest to the geometric center of the cluster. We compute the IoU between points in the box and the ones in the cluster. We also use the class labels of the box to categorize each cluster. If IoU is zero, we categorize the detected cluster as "Other." We use the class labels for evaluation purpose only and report the evaluation results in Table 3.

Box count	Car	Pedestrian	Cyclist	Other
Neural-SF	1027229	729275	29178	348452
SSL-SF	731480	631745	28369	543206
GT	1161019	1427211	42411	-
Mean IoU	Car	Pedestrian	Cyclist	Other
Neural-SF	70.3	95.5	96.5	-
SSL-SF	67.4	90.0	91.6	-

Table 3: Object trace detection results.

Analysis. Table 3 provides object trace detection results; Figure 5 qualitatively compares our detected object traces using Neural-SF to the ground truth object points. Both algorithms achieve reasonable performance finding object traces from point cloud sequences. Neural-SF outperforms SSL-SF, possibly due to the joint estimation of motion among all frames, which provides robustness against false positive and false negative motions and promotes smoothness of motion.

5.2 Unsupervised Object Detection Results

Here, we evaluate the performance of our single-frame object detector trained with minimal class labels. We use object traces from Neural-SF, due to their superior quality. Since multiple iterations of label propagation are involved (§4), we report the performance for both our final model and the intermediate models after each label propagation iteration; we also try to remove motion segmentation (task I) and repeat the procedure for object detection (task II) only.

Evaluation protocol. We report L1 and L2 Average Precision (AP) on the validation split of the Waymo dataset for vehicles, pedestrians, and cyclists. We use two sets of IoU thresholds to compute AP for each object class: $\{0.6, 0.7\}$ for vehicles, $\{0.4, 0.5\}$ for pedestrians, and $\{0.4, 0.5\}$ for cyclists. One of the IoU thresholds for each class is identical to the standard choice. See Table 4.

Analysis. Our unsupervised single-frame object detector works well for all classes (see Table 2). Among all three object classes, we achieved the highest precision on cyclist class, which reflects the quality and coverage of our detected object traces for each object class reported §5.1. Empiricailly, we found that adding more iterations of label propagation do not improve overall performance. A possible reason is that the label propagation algorithm is sensitive to hyper-parameters.

5.3 Self-supervised Object Detection Results

In this section, we compare with two state-of-the-art self-supervised learning approaches: PointContrast [17] and DepthContrast [16]. These two methods work on single-frame point clouds but do not test on the Waymo Open dataset. We implement these two methods with a CenterPoint [52] pipeline. For ablation study, we train our model with three options: 1) (task-I) only task I's loss is used, 2) (task-II) only task II's loss is used, 3) (all) the sum of both tasks' loss is used.

Following the self-supervised learning routine, we split our training set into two parts and use all training point cloud sequences to pretrain a feature extraction module without using any labels. Then, we fine-tune the pretrained feature extraction module on 10% of the training point cloud sequences. The evaluation metrics follow §5.2; we use standard IoU thresholds for this experiment, i.e., 0.7, 0.5 and 0.5 for vehicle, pedestrian and cyclist, respectively.

Analysis. Table 4 summarizes our results. PointContrast and DepthContrast improve overall AP by 0.6% and 0.2%, resp. Our self-supervised tasks achieved 0.8%, 1.9% and 2.6% improvement for task I (motion segmentation), task II (object detection), and all tasks, resp. Among all three classes, we achieved the highest improvement on cyclists due to quality of the detected object traces, agreeing with the results from §5.2 and §5.1.

	Vehicle	Pedestrian	Cyclist
(10% train)	60.6	60.7	65.4
PointContrast	61.3	61.3	66.0
DepthContrast	60.9	60.7	65.7
Ours-task-I	61.5	61.4	66.3
Ours-task-II	62.2	62.6	67.6
Ours-all	63.3	63.0	68.4
(100% train)	66.5	67.7	69.3

Table 4: Single-frame object detection results for self-supervised learning.

6 Discussion and Conclusion

Our object trace detection algorithm reliably extracts objects that consistently and smoothly move in a point cloud sequence. These easily-extracted moving object traces provide critical information for downstream object detection without supervision, uncovered using our self-supervised tasks. Our design choices differ from other auto-labeling approaches, emphasizing quality over quantity of the pseudo-labels. Even though some class labels are needed to achieve state-of-the-art class-aware object detection performance, our work reveals the power and ease of obtaining high-precision/low-coverage pseudo-labels to train complex 3D shape analysis tasks like object detection.

Limitations and Future Work. Our method requires a minimal amount of categorical labels to distinguish between different objects; we view this requirement as sensible, in that the *type* of moving object (vehicle, pedestrian, cyclist) requires semantic knowledge. Moreover, the painstaking process of annotating object bounding boxes in typical 3D supervision is not needed in our setting: we just need a class label for our pre-detected object boxes (one of three discrete options, rather than a position of a box in 3D). If such supervision is removed, a candidate replacement of the learned object classifiers might be to cluster the moving objects based on their geometry alone; our attempts at this unsupervised approach decreased performance. Incorporating self-supervised or unsupervised object classifier models might be a promising direction to better automate this pipeline.

Our method focuses on movable objects like pedestrians, cyclists, and vehicles, since other classes will not be captured by object trace detection. Different pretext tasks are needed for detecting static object classes. One could consider spatio-temporal structures and complementary views.

Acknowledgments

The MIT Geometric Data Processing group acknowledges the generous support of Army Research Office grants W911NF2010168 and W911NF2110293, of Air Force Office of Scientific Research award FA9550-19-1-031, of National Science Foundation grants IIS-1838071 and CHS-1955697, from the CSAIL Systems that Learn program, from the MIT–IBM Watson AI Laboratory, from the Toyota–CSAIL Joint Research Center, and from a gift from Adobe Systems. The Toyota Research Institute provided funds to support this work.

References

[1] P. Sun, H. Kretzschmar, X. Dotiwalla, A. Chouard, V. Patnaik, P. Tsui, J. Guo, Y. Zhou, Y. Chai, B. Caine, et al. Scalability in perception for autonomous driving: Waymo open dataset. In *Proceedings of the IEEE/CVF Conference on Computer Vision and Pattern Recognition*, 2020.

[2] H. Caesar, V. Bankiti, A. H. Lang, S. Vora, V. E. Liong, Q. Xu, A. Krishnan, Y. Pan, G. Baldan, and O. Beijbom. nuscenes: A multimodal dataset for autonomous driving. In *Proceedings of the IEEE/CVF Conference on Computer Vision and Pattern Recognition*, 2020.

[3] Y. Wang, A. Fathi, J. Wu, T. A. Funkhouser, and J. M. Solomon. Multi-frame to single-frame: Knowledge distillation for 3d object detection. *ECCV Workshop on Perception for Autonomous Driving*, 2020.

[4] C. Luo, X. Yang, and A. Yuille. Self-supervised pillar motion learning for autonomous driving. In *Proceedings of the IEEE/CVF Conference on Computer Vision and Pattern Recognition*, 2021.

[5] B. Mersch, X. Chen, J. Behley, and C. Stachniss. Self-supervised point cloud prediction using 3d spatio-temporal convolutional networks. In *5th Annual Conference on Robot Learning*, 2021.

[6] Y. Shi, X. Cao, and B. Zhou. Self-supervised learning of part mobility from point cloud sequence. In *Computer Graphics Forum*, 2021.

[7] H. Wang, L. Yang, X. Rong, J. Feng, and Y. Tian. Self-supervised 4d spatio-temporal feature learning via order prediction of sequential point cloud clips. In *Proceedings of the IEEE/CVF Winter Conference on Applications of Computer Vision*, 2021.

[8] S. Yuan, X. Li, and Y. Fang. Deeptracking-net: 3d tracking with unsupervised learning of continuous flow. *arXiv preprint arXiv:2006.13848*, 2020.

[9] D. Rempe, T. Birdal, Y. Zhao, Z. Gojcic, S. Sridhar, and L. J. Guibas. Caspr: Learning canonical spatiotemporal point cloud representations. In *Advances in Neural Information Processing Systems (NeurIPS)*, 2020.

[10] S. A. Baur, D. J. Emmerichs, F. Moosmann, P. Pinggera, B. Ommer, and A. Geiger. SLIM: Self-supervised LiDAR scene flow and motion segmentation. In *Proceedings of the IEEE/CVF International Conference on Computer Vision*, 2021.

[11] C. R. Qi, Y. Zhou, M. Najibi, P. Sun, K. Vo, B. Deng, and D. Anguelov. Offboard 3d object detection from point cloud sequences. In *Proceedings of the IEEE/CVF Conference on Computer Vision and Pattern Recognition*, 2021.

[12] I. Bogoslavskyi and C. Stachniss. Fast Range Image-Based Segmentation of Sparse 3D Laser Scans for Online Operation. In *International Conference on Intelligent Robots and Systems (IROS)*, 2016. URL `http://www.ipb.uni-bonn.de/pdfs/bogoslavskyi16iros.pdf`.

[13] I. Bogoslavskyi and C. Stachniss. Efficient online segmentation for sparse 3d laser scans. *PFG–Journal of Photogrammetry, Remote Sensing and Geoinformation Science*, 85(1):41–52, 2017.

[14] P. M. Chu, S. Cho, Y. W. Park, and K. Cho. Fast point cloud segmentation based on flood-fill algorithm. *IEEE International Conference on Multisensor Fusion and Integration for Intelligent Systems (MFI)*, pages 656–659, 2017.

[15] J. Sauder and B. Sievers. Self-supervised deep learning on point clouds by reconstructing space. In *Advances in Neural Information Processing Systems (NeurIPS)*, 2019.

[16] Z. Zhang, R. Girdhar, A. Joulin, and I. Misra. Self-supervised pretraining of 3d features on any point-cloud. In *Proceedings of the IEEE/CVF International Conference on Computer Vision*, 2021.

[17] S. Xie, J. Gu, D. Guo, C. R. Qi, L. Guibas, and O. Litany. Pointcontrast: Unsupervised pre-training for 3d point cloud understanding. In *The European Conference on Computer Vision*, 2020.

[18] Y. Liu, L. Yi, S. Zhang, Q. Fan, T. A. Funkhouser, and H. Dong. P4Contrast: Contrastive learning with pairs of point-pixel pairs for RGB-D scene understanding. *ArXiv*, abs/2012.13089, 2020.

[19] Y. Liu, Q. Fan, S. Zhang, H. Dong, T. A. Funkhouser, and L. Yi. Contrastive Multimodal Fusion with TupleInfoNCE. *ArXiv*, abs/2107.02575, 2021.

[20] H. Tian, Y. Chen, J. Dai, Z. Zhang, and X. Zhu. Unsupervised object detection with lidar clues. In *Proceedings of the IEEE/CVF Conference on Computer Vision and Pattern Recognition*, 2021.

[21] Y. Zhou and O. Tuzel. Voxelnet: End-to-end learning for point cloud based 3d object detection. In *Proceedings of the IEEE/CVF Conference on Computer Vision and Pattern Recognition*, 2018.

[22] Y. Wang and J. M. Solomon. Object dgcnn: 3d object detection using dynamic graphs. In *Advances in Neural Information Processing Systems*, 2021.

[23] A. H. Lang, S. Vora, H. Caesar, L. Zhou, J. Yang, and O. Beijbom. Pointpillars: Fast encoders for object detection from point clouds. In *Proceedings of the IEEE/CVF Conference on Computer Vision and Pattern Recognition*, 2019.

[24] G. P. Meyer, A. Laddha, E. Kee, C. Vallespi-Gonzalez, and C. K. Wellington. Lasernet: An efficient probabilistic 3d object detector for autonomous driving. In *Proceedings of the IEEE/CVF Conference on Computer Vision and Pattern Recognition*, 2019.

[25] L. Fan, X. Xiong, F. Wang, N. Wang, and Z. Zhang. Rangedet: In defense of range view for lidar-based 3d object detection. In *Proceedings of the IEEE/CVF International Conference on Computer Vision*, 2021.

[26] Y. Zhou, P. Sun, Y. Zhang, D. Anguelov, J. Gao, T. Ouyang, J. Guo, J. Ngiam, and V. Vasudevan. End-to-End Multi-View Fusion for 3D Object Detection in LiDAR Point Clouds. In *The Conference on Robot Learning (CoRL)*, 2019.

[27] Y. Wang, A. Fathi, A. Kundu, D. Ross, C. Pantofaru, T. Funkhouser, and J. Solomon. Pillar-based object detection for autonomous driving. In *The European Conference on Computer Vision*, 2020.

[28] Z. Zhang, B. Sun, H. Yang, and Q.-X. Huang. H3DNet: 3D Object Detection Using Hybrid Geometric Primitives. In *The European Conference on Computer Vision*, 2020.

[29] W. Luo, B. Yang, and R. Urtasun. Fast and furious: Real time end-to-end 3d detection, tracking and motion forecasting with a single convolutional net. In *Proceedings of the IEEE/CVF Conference on Computer Vision and Pattern Recognition*, pages 3569–3577, 2018.

[30] P. Hu, J. Ziglar, D. Held, and D. Ramanan. What you see is what you get: Exploiting visibility for 3d object detection. In *Proceedings of the IEEE/CVF Conference on Computer Vision and Pattern Recognition*, 2020.

[31] J. Yin, J. Shen, C. Guan, D. Zhou, and R. Yang. Lidar-based online 3d video object detection with graph-based message passing and spatiotemporal transformer attention. In *Proceedings of the IEEE/CVF Conference on Computer Vision and Pattern Recognition*, 2020.

[32] R. Huang, W. Zhang, A. Kundu, C. Pantofaru, D. A. Ross, T. Funkhouser, and A. Fathi. An lstm approach to temporal 3d object detection in lidar point clouds. In *European Conference on Computer Vision*, 2020.

[33] J. Ku, M. Mozifian, J. Lee, A. Harakeh, and S. Waslander. Joint 3d proposal generation and object detection from view aggregation. In *The International Conference on Intelligent Robots and Systems (IROS)*, 2018.

[34] X. Chen, H. Ma, J. Wan, B. Li, and T. Xia. Multi-view 3d object detection network for autonomous driving. In *Proceedings of the IEEE/CVF Conference on Computer Vision and Pattern Recognition*, 2016.

[35] D. Xu, D. Anguelov, and A. Jain. Pointfusion: Deep sensor fusion for 3d bounding box estimation. In *Proceedings of the IEEE/CVF Conference on Computer Vision and Pattern Recognition*, 2018.

[36] C. R. Qi, W. Liu, C. Wu, H. Su, and L. J. Guibas. Frustum pointnets for 3d object detection from rgb-d data. In *Proceedings of the IEEE/CVF Conference on Computer Vision and Pattern Recognition*, 2018.

[37] B. Yang, M. Liang, and R. Urtasun. Hdnet: Exploiting hd maps for 3d object detection. In *The Conference on Robot Learning (CORL)*, 2018.

[38] M. Liang, B. Yang, Y. Chen, R. Hu, and R. Urtasun. Multi-task multi-sensor fusion for 3d object detection. In *Proceedings of the IEEE/CVF Conference on Computer Vision and Pattern Recognition*, 2019.

[39] K. Wong, S. Wang, M. Ren, M. Liang, and R. Urtasun. Identifying unknown instances for autonomous driving. In *The Conference on Robot Learning (CORL)*, 2019.

[40] A. Dai, A. X. Chang, M. Savva, M. Halber, T. Funkhouser, and M. Nießner. Scannet: Richly-annotated 3d reconstructions of indoor scenes. In *Proceedings of the IEEE/CVF Conference on Computer Vision and Pattern Recognition*, pages 5828–5839, 2017.

[41] S. Choi, Q.-Y. Zhou, S. Miller, and V. Koltun. A Large Dataset of Object Scans. *arXiv:1602.02481*, 2016.

[42] J. Behley, M. Garbade, A. Milioto, J. Quenzel, S. Behnke, C. Stachniss, and J. Gall. Semantickitti: A dataset for semantic scene understanding of lidar sequences. In *Proceedings of the IEEE/CVF International Conference on Computer Vision*, 2019.

[43] A. Geiger, P. Lenz, C. Stiller, and R. Urtasun. Vision meets robotics: The kitti dataset. *The International Journal of Robotics Research*, 32(11), 2013.

[44] C. Choy, J. Gwak, and S. Savarese. 4d spatio-temporal convnets: Minkowski convolutional neural networks. In *Proceedings of the IEEE/CVF Conference on Computer Vision and Pattern Recognition*, 2019.

[45] X. Liu, M. Yan, and J. Bohg. Meteornet: Deep learning on dynamic 3d point cloud sequences. In *Proceedings of the IEEE/CVF International Conference on Computer Vision*, 2019.

[46] J. Shi and J. Malik. Normalized cuts and image segmentation. *IEEE Transactions on Pattern Analysis and Machine Intelligence*, 22(8):888–905, 2000.

[47] X. Li, J. Kaesemodel Pontes, and S. Lucey. Neural scene flow prior. In *Advances in Neural Information Processing Systems*, 2021.

[48] H. Mittal, B. Okorn, and D. Held. Just go with the flow: Self-supervised scene flow estimation. In *Proceedings of the IEEE/CVF Conference on Computer Vision and Pattern Recognition*, 2020.

[49] X. Weng and K. Kitani. A baseline for 3d multi-object tracking. *arXiv preprint arXiv:1907.03961*, 1(2):6, 2019.

[50] V. Nair and G. E. Hinton. Rectified linear units improve restricted boltzmann machines. In *International conference on machine learning*, 2010.

[51] S. Ioffe and C. Szegedy. Batch normalization: Accelerating deep network training by reducing internal covariate shift. In *International conference on machine learning*, pages 448–456. PMLR, 2015.

[52] T. Yin, X. Zhou, and P. Krahenbuhl. Center-based 3d object detection and tracking. In *Proceedings of the IEEE/CVF Conference on Computer Vision and Pattern Recognition*, 2021.

[53] H. Zhao, L. Jiang, J. Jia, P. H. Torr, and V. Koltun. Point transformer. In *Proceedings of the IEEE/CVF International Conference on Computer Vision*, 2021.

[54] T. Yin et al. Center-based 3D Object Detection and Tracking. `https://github.com/tianweiy/CenterPoint`, 2021.

[55] Y. Yan et al. SpConv: Spatially Sparse Convolution Library. `https://github.com/traveller59/spconv`, 2021.

A Point Cloud Sequence Preprocessing

Our approach is similar to [13], except that we use the entire point cloud sequence instead of range images to reconstruct the ground plane.

To remove points on the ground, we observe that the ground plane is a smooth surface that approximately aligns with the x-y plane. We solve an optimization problem to estimate the ground height $h_{i,j}$ at a set of 2D grid cells with centers $(x_{i,j}, y_{i,j})$ on the x-y plane; our implementation uses a 1000×1000 grid. We denote the height of the k-th input point as z_k, the set of points in grid cell (i,j) as $G_{i,j}$, and the neighboring cells of cell (i,j) as $\mathcal{N}_{i,j}$. The optimization problem is

$$\min_{\boldsymbol{h}} \sum_i \left[\frac{1}{|G_i|} \sum_{j \in G_i} \|h_i - z_j\|_1 + \frac{\lambda}{2} \sum_{(i',j') \in \mathcal{N}_{i,j}} \|2h_{i,j} - h_{i',j'} - h_{2i-i',2j-j'}\|_1 \right]. \tag{4}$$

We use a piecewise-linear first term to tolerate noisy inputs. We solve (4) using gradient descent, with $\lambda = 0.1$ and stopping condition $\|\Delta \boldsymbol{h}\|_\infty < 0.01$ m. Then, point $j \in G_i$ is removed if $z_j < h_i + \delta$; our experiments use $\delta = 0.5$ m. An example of the resulting point cloud after ground plane removal can be seen in Fig. 3b.

B Object Trace Tracking Algorithm

For tracking object trace, we begin with the geometric center of the object cluster and zero velocity and iteratively register the object cluster to the adjacent frames; see Algorithm 1. We use two stopping conditions for trace tracking to reject large average registration errors and large acceleration magnitudes, with thresholds $\sigma_0 = 1.0$ m and $\sigma_1 = 3.0\text{m/s}^2$.

For each object cluster, the output of tracking is a sequence of rigid transformations that transforms the cluster across frames. We collect the points that are geometrically close to any of the transformed object cluster points within distance $r = 0.3$ m. If the points of two object traces overlap by at least 10% intersection over union (IoU), we reject the one with the smaller number of points. Figure 3(d) shows example extracted object traces.

Algorithm 1 Object Trace Tracking from s-th to t-th frame.

```
Input: Point cloud sequence $\{P_i\}$, object cluster proposal $C_s \subset P_s$, kalman filter KF, registration error threshold $\sigma_0$, acceleration threshold $\sigma_1$.
1. Initialize KF with state (avg($C_s$), $\mathbf{0}$).
2. $\mathcal{T} \leftarrow \{C_s\}$, $\boldsymbol{v}^- \leftarrow \mathbf{0}$.
for $i = s+1$ to $t$ do
    3. $C \leftarrow C_{i-1} +$ KF.CurrentVelocity().
    # get deformed points, registration error
    4. $C_i, \sigma \leftarrow$ Rigid-ICP$(C, P_i)$
    5. $\boldsymbol{v} \leftarrow$ avg$(C_i)$ − avg$(C_{i-1})$
    if $\|\boldsymbol{v} - \boldsymbol{v}^-\| > \sigma_1$ or $\sigma > \sigma_0$ then
        BREAK
    end if
    7. KF.UpdateState(avg($C_i$))
    8. $\mathcal{T} \leftarrow \mathcal{T} \cup \{C_i\}$, $\boldsymbol{v}^- \leftarrow \boldsymbol{v}$
end for
Output: $\mathcal{T}$
```

C Details on 3D bounding box estimation

Here we elaborate the loss functions d_1 and d_2 from (3). We first unpack the box attribute vector $\boldsymbol{b}_i \in \mathbb{R}^7$ as $\boldsymbol{c}_i \in \mathbb{R}^3$, $\boldsymbol{s}_i \in \mathbb{R}^3$ and θ_i, representing box center, box size and orientation, respectively. Since the box size is fixed for each trace, d_1 is defined as

$$d_1(b_i, b_j) = \gamma_1 \|c_i - c_j\|^2 + \|\sin(\theta_i) - \sin(\theta_j)\|^2 + \|\cos(\theta_i) - \cos(\theta_j)\|^2 \tag{5}$$

where γ_1 is set to 0.1.

For the definition of d_2, we define outward the normal vector $\boldsymbol{n}_{i,1} \ldots \boldsymbol{n}_{i,6}$ and face center $\boldsymbol{c}_{i,1}, \ldots \boldsymbol{c}_{i,6}$ for the faces of the 3D bounding box represented by b_i:

$$d_2(\boldsymbol{b}_i, C_i) = \frac{\gamma_2}{|C_i|} \sum_{p \in C_i} \sum_{k=1}^{6} \max(\langle \boldsymbol{p} - \boldsymbol{c}_{i,k}, \boldsymbol{n}_{i,k} \rangle, 0), \tag{6}$$

where γ_2 is set to 0.1 to make sure that this loss function can tolerate a small fraction of outlier points in the point clusters.

D Details on Label Propagation from moving to static objects

Since the goal of label propagation is to generate 3D bounding boxes for static objects using the distilled knowledge about the appearance of moving objects, we apply the trained single-frame object detector on all training point clouds. Specifically, the input to the label propagation algorithm is a set of predicted bounding boxes in a point cloud sequence. And we aim to find more bounding boxes purely based on geometric appearance to improve generalization to static objects. To further enforce consistency, we track the bounding boxes using the exact algorithm in Weng and Kitani [49] while looking for bounding boxes that do not move across temporally adjacent frames. Specifically, we build a spatial-temporal graph of bounding boxes and connect a pair of bounding boxes only if 1) they are overlapping with IoU greater than 0.5, 2) the translation between box centers is not more than 0.3m and 3) they are classified as the same class. We then collect all chain of bounding boxes that are at least 10 frames long, and add all collected 3D bounding boxes to the training set. We apply an iterative algorithm that takes chains of bounding boxes without replacement, and stops when no more chains satisfying all three conditions can be found.

We visualize the intermediate results of our label propagation stated in §4.2 in figure 6.

E Kalman Filter Algorithmic Components

We adapt standard definition[2] to derive our version of Kalman filter, which tracks a moving object point cluster across a sequence of temporally consecutive frames of point cloud.

Kalman filter contains three algorithmic components, i.e. initialization, prediction and update. In algorithm 1, we demonstrated how to use each component of Kalman filter. In below, we illustrate each component separately.

Initialization. Each Kalman filter is initialized with a 6D state vector $\boldsymbol{x} = (\boldsymbol{c}, \boldsymbol{v})$, indicating a 3D location and a velocity. It is also parameterized with three hyper-parameters: Δ_t, a, σ, indicating elapsed time between frames, maximum acceleration, and standard deviation of measurement noise, respectively. During initialization, we set

$$H \leftarrow (I_3; \quad 0) \in \mathbb{R}^{3\times 6}, \quad A \leftarrow \begin{pmatrix} I_3 & I_3 \\ & I_3 \end{pmatrix}, \quad Q \leftarrow a \begin{pmatrix} \frac{\Delta_t^4}{4} I_3 & \frac{\Delta_t^3}{2} I_3 \\ \frac{\Delta_t^3}{2} I_3 & \Delta_t^2 I_3 \end{pmatrix}$$
$$R \leftarrow \sigma I_3, \quad P \leftarrow I_6$$

Prediction. This is where we predict the next 3D location. Specifically, we set

$$x \leftarrow A\boldsymbol{x}, \quad P \leftarrow APA^T + Q \tag{7}$$

Update. When we observe the next observed location $\boldsymbol{z}$, we update state vectors. Specifically, we set

$$S \leftarrow HPH^T + R \tag{8}$$
$$K \leftarrow PH^T S^{-1} \tag{9}$$
$$x \leftarrow x + K(z - Hx) \tag{10}$$
$$P \leftarrow (I_6 - KH)P \tag{11}$$
$$\tag{12}$$

[2] https://en.wikipedia.org/wiki/Kalman_filter

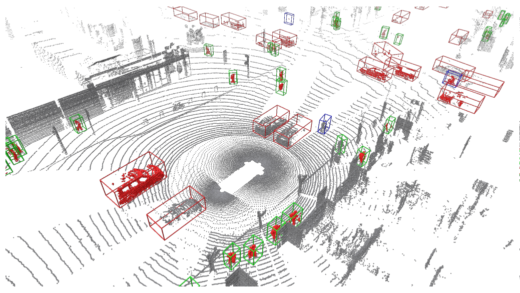
(a) Ground Truth

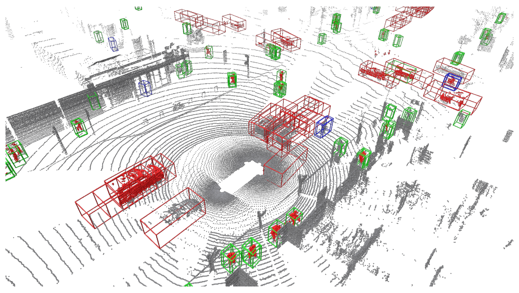
(b) Before Propagation

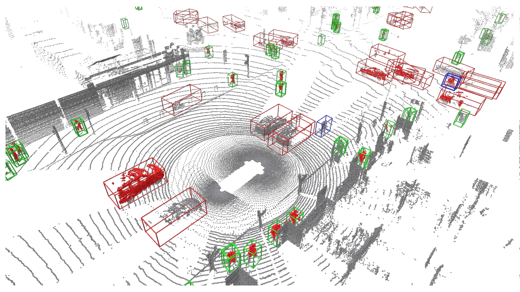
(c) First Iteration

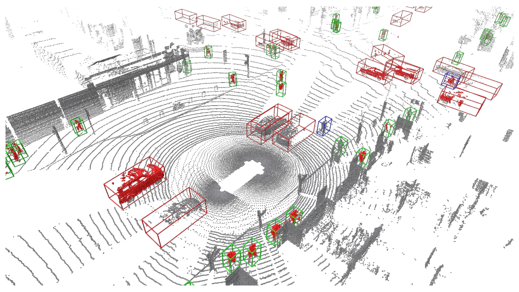
(d) Second Iteration

Figure 6: Qualitative results of our label propagation algorithm. The top-left figure shows the ground truth bounding boxes, with moving object points in highlighted in red and boxes colored based on their object class (red: Vehicle, green: pedestrian, blue: cyclist). The next three figures shows the effect of label propagation, essentially we are making more and more correct predictions of bounding boxes on static objects. The second iteration corresponds to the prediction of our final object detector.